

Investigating the Reaction Dynamics of Dicarbon
Molecules, $C_2(X^1\Sigma_g^+/a^3\Pi_u)$, with Acetylene, $C_2H_2(X^1\Sigma_g^+)$

Xibin Gu,¹ Ying Guo,¹ Alexander M. Mebel,² Ralf I. Kaiser^{1*}

¹ *Department of Chemistry, University of Hawai'i at Manoa, Honolulu, HI 96822.*

² *Department of Chemistry and Biochemistry, Florida International University, Miami, FL 33199.*

ABSTRACT

The reaction of dicarbon molecules in their electronic ground, $C_2(X^1\Sigma_g^+)$, and first excited state, $C_2(a^3\Pi_u)$, with acetylene, $C_2H_2(X^1\Sigma_g^+)$, to form the 1,3-butadiynyl, $C_4H(X^2\Sigma^+)$, plus a hydrogen atom was investigated under single collision conditions at six different collision energies between 10.6 kJmol^{-1} and 47.5 kJmol^{-1} . Augmented by electronic structure calculations, dicarbon was found to react with acetylene on the 1A surface without entrance barrier via complex formation through an addition process involving s-INT1 and/or s-INT2 intermediates. The latter undergoes ring opening to the diacetylene molecule s-INT3 which decomposes via a loose exit transition state by an emission of a hydrogen atom to form the 1,3-butadiynyl radical $C_4H(X^2\Sigma^+)$; the overall reaction was found to be exoergic by about 33 kJmol^{-1} . The $D_{\infty h}$ symmetry of the decomposing diacetylene intermediate results in collision-energy invariant, isotropic (flat) center-of-mass angular distributions of this microchannel. On the triplet surface, the reaction involves three feasible addition complexes t-INT1, t-INT2, and t-INT3. Following the 3A surface, the reaction strongly depends on the impact parameter. Lower collision energies go hand-in-hand with larger impact parameters and hence the formation of t-INT2 and t-INT3 as the initial collision complex, whereas with increasing collision energy, smaller impact parameters become more important to form t-INT1. These dynamics result in forward-scattered contour plots of the heavy 1,3-butadiynyl radical $C_4H(X^2\Sigma^+)$ at lower collision energies; as the collision energy rises, the distributions switch to a pronounced backward scattering. The definite detection of the 1,3-butadiynyl radical, $C_4H(X^2\Sigma^+)$, as the sole reaction product of the dicarbon versus hydrogen exchange pathway in the bimolecular collision with acetylene represents a single, one-step mechanism to build up a hydrogen-deficient organic radical and can account for the hitherto unexplained formation of the 1,3-butadiynyl radical in extreme environments like combustion flames, cold molecular clouds, and outflows of carbon stars.

1. Introduction

The linear 1,3-butadiynyl radical in its $^2\Sigma^+$ electronic ground state holds the global minimum on the C_4H potential energy surface (PES) (Figure 1). In recent years, this hydrogen-deficient molecule has received considerable attention due to its potential importance as a precursor to polycyclic aromatic hydrocarbons (PAHs) and possibly to fullerenes¹ in the interstellar medium,^{2,3,4,5} in hydrocarbon-rich atmospheres of planets and their moons,^{6,7} and in combustion processes.^{8,9,10} The butadiynyl radical was first synthesized in 1975 in low temperature (4 K) argon and neon noble gas matrices.¹¹ Generated via ultraviolet photolysis of diacetylene (C_4H_2 ; $X^1\Sigma_g^+$), the carbon-carbon stretching mode of the triple bond was detected in the infrared regime at 2060 cm^{-1} .¹¹ Very recently, the carbon-hydrogen stretching mode was also observed in solid argon at 3307 cm^{-1} , whereas the carbon-carbon stretching vibration of the single bond was assigned to be at $960 \pm 50\text{ cm}^{-1}$.^{12,13} The position of the doubly degenerate skeleton bending mode is still under debate and suggested to lie between 131 and 226 cm^{-1} .^{14,15} The electron spin resonance (ESR) spectrum exhibits a proton hyperfine splitting of 16.5 MHz ; the spin doubling constant was estimated to be $+0.0006\text{ cm}^{-1}$. Note that the first excited state of the 1,3-butadiynyl radical, $A^2\Pi$, is only 5.6 kJmol^{-1} above the ground state,¹⁵ whereas the $B^2\Pi$ state was found to be higher by 287.5 kJmol^{-1} than the $^2\Sigma^+$ electronic ground state.¹⁵ A recent laser induced fluorescence (LIF) spectrum of the 1,3-butadiynyl radical in a supersonic free jet expansion confirmed the existence of a low lying $A^2\Pi$ electronically excited state exhibiting a strong vibronic mixing with the $^2\Sigma^+$ ground state.¹⁶ The fluorescence time profile consisted of two decay components via internal conversion: a fast decay ($\tau \approx 20\text{ ns}$) and a slow component with complex quantum beats ($\tau \approx 3 - 4\text{ }\mu\text{s}$). These experimentally determined energies of the first excited state gain additional support from recent electronic structure calculations employing multireference configuration interaction; these computations suggest an energy difference of about 3.4 kJmol^{-1} .¹⁷ These studies were supplemented by Thaddeus et al.¹⁸ and Cernicharo et al.¹⁹ recording millimeter wave spectra of the 1,3-butadiynyl radical. The authors determined the rotational constant B to be 4759 MHz and bond lengths of 122.7 pm (C1-C2), 135.9 pm (C2-C3), 121.1 pm (C3-C4), and 105.5 pm (C4-H). These data suggest the existence of two carbon-carbon triple bonds (C1-C2; C3-C4); the C2-C3 bond is shorter than a typical carbon-carbon single bond of about 154 pm in ethane but in close agreement with the distance of a carbon-carbon double bond in ethylene (134 pm);

likewise, the carbon-hydrogen bond length is similar to the acetylenic carbon-hydrogen bond length.^{20,21} The dipole moment of ground state 1,3-butadiynyl was determined to be about 0.87 Debye,²² whereas its enthalpy of formation was calculated to be $754 \pm 4 \text{ kJmol}^{-1}$.²³

These spectroscopic data also assisted in identification of the butadiynyl radical in extreme environments. In the circumstellar envelope of the dying carbon star IRC+10216 (CW Leo),²⁴ four emission doublets in the millimeter wave spectrum were identified as the $N = 9 \rightarrow 8$, $10 \rightarrow 9$, $11 \rightarrow 10$, and $12 \rightarrow 11$ rotational transitions of the $\text{HCCCC}(X^2\Sigma^+)$ radical.²⁵ A rotational constant of $B = 4758.48 \pm 0.10 \text{ MHz}$ was derived as well. The strengths of the emission lines suggest column densities in the range of 4×10^{14} and $3 \times 10^{15} \text{ cm}^{-2}$. A recent survey limited the column density to $5.6 - 9.4 \times 10^{15} \text{ cm}^{-2}$ – one order of magnitude higher than the ubiquitous C_3H radical and about 25 % more abundant than the ethynyl radical ($\text{HCC}; X^2\Sigma^+$).²⁶ Millimeter data from the BIMA (Berkeley-Illinois-Maryland Association) interferometer clearly showed that the butadiynyl molecule is actually distributed in a shell surrounding the central star, with little emission from the inner envelope.²⁷ Peak abundances of 1.8×10^{-6} with respect to molecular hydrogen at a radius of $2.5 \times 10^{14} \text{ m}$ were reported. The derived C_4H distribution was compared with the prediction from photochemical models assuming all the butadiynyl radicals originate from photolysis of diacetylene ($\text{C}_4\text{H}_2; X^1\Sigma_g^+$). Here, the models were found to underestimate the astronomical observations by a factor of five suggesting that not all production rates to the butadiynyl molecule have been incorporated in the chemical models of IRC+10216.²⁸

Following the detection of the butadiynyl radical in the circumstellar envelope of IRC+10216, Irvine and coworkers identified the linear C_4H species based on the hyperfine-resolved $N = 3 \rightarrow 2$ transition in the Taurus Molecular Cloud (TMC-1) – a cold molecular cloud in which gas phase molecules hold typical averaged translational temperatures of about 10 K.^{29,30} Abundance ratios at the TMC-1 peak suggest that the butadiynyl radical holds only slightly lower concentrations as the ethynyl radical $\text{HCC}(X^2\Sigma^+)$, i.e. fractional abundances of 2×10^{-8} with respect to molecular hydrogen.^{31,32,33,34} However, the observed abundances cannot be reproduced by gas phase models including solely ion-molecule reaction schemes.^{35,36} The observation of butadiynyl deep inside TMC-1 correlates nicely with its detection in photon dominated region.³⁷ Photon dominated

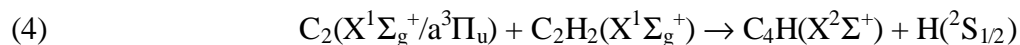
regions (PDRs) such as the edge of the Horsehead Nebula (B33) are surface layers of interstellar molecular clouds exposed to intense fluxes of far ultraviolet photons; as a matter of fact, each molecular cloud has outer, photon dominated regions.³⁷ The authors suggested a photodestruction of small carbonaceous grains (photo erosion) and possibly polycyclic aromatic hydrocarbon molecules to produce hydrogen-deficient radical fragments such as the butadiynyl radical in significant amounts.³⁸ Subsequent scans verified these conclusions. In the Orion Bar and Horsehead Nebula, the microwave emissions of the butadiynyl radicals spatially correlate with the emission of aromatic infrared bands such as the 3.3 μm and 7.0 μm features.^{39,40} Note that the butadiynyl radical has also been suggested as an important building block in the solar-photon driven photochemical processing of planetary atmospheres.^{41,42} Here, models postulate that photochemistry of diacetylene should yield significant fractional abundances of butadiynyl species in the atmospheres of Jupiter,⁴³ Saturn,⁴⁴ Uranus,⁴⁵ Neptune,⁴⁶ and Saturn's moon Titan.⁴⁷ The HCCC ($X^2\Sigma^+$) radical was also been identified as a constituent in the coma of comet P/Halley.⁴⁸

The chemistry of oxygen-deficient combustion flames^{49,50} is astonishingly similar to the chemical evolution of the circumstellar envelopes of carbon stars.^{51,52} Both in extraterrestrial setting and in combustion flames,⁵³ the butadiynyl radical has been suggested as a precursor to complex polycyclic aromatic hydrocarbons (PAHs) formed at temperatures between 2000 – 5000 K⁵⁴ and possibly fullerenes like C_{60} and C_{82} .^{55,56,57} The majority of all combustion models suggest a stepwise formation of complex PAHs via acetylene⁵⁸ and benzene⁵⁹ involving radicals such as butadiynyl.⁶⁰ Since the formation of small, hydrogen deficient carbon clusters such as the $C_4H(X^2\Sigma^+)$ radical is thought to be strongly linked to the synthesis of polycyclic aromatic hydrocarbons and ultimately to carbonaceous nanoparticles and soot production in oxygen-poor combustion flames,⁶⁰ it is imperative to actually elucidate how these radical precursors are actually formed in combustion flames from the 'bottom up' in bimolecular collisions involving simple atoms and radicals.⁶¹ Here, carbonaceous nanoparticles are commonly referred to as soot and are often associated with incomplete combustion processes.^{62,63} Soot is primarily composed of nanometer-sized stacks of planar layers of carbon atoms. These layers can be characterized as fused benzene rings and are likely formed via agglomeration of polycyclic aromatic hydrocarbons.⁶⁴ Once liberated into the ambient environment, soot particles in respirable size of 10-100 nm can be transferred into the lungs by inhalation and are strongly implicated in the degradation

of human health,⁶⁵ particularly due to their high carcinogenic risk potential. PAHs and carbonaceous nanoparticles are also serious water pollutants and bioaccumulate in the fatty tissue of living organisms. Together with leafy vegetables, where PAHs and soot deposit easily, they have been further linked to food poisoning, liver lesions, and tumor growth. Even smaller soot particles of 1–10 nm can be transported to high altitudes and influence the atmospheric chemistry.⁶⁶ These particles act as condensation nuclei for water ice, accelerate the degradation of ozone, and could lead ultimately to an increased rate of skin cancer on Earth and possibly to a reduced harvest of crops. The crucial role of nanodiamonds in chemical vapor deposition on the industrial scale should be also noted.⁶⁷

However, despite the importance of the 1,3-butadiynyl radical in astrochemistry⁶⁸ and in combustion processes as a precursor to polycyclic aromatic hydrocarbon (PAH) molecules, the question ‘How is the 1,3-butadiynyl radical actually formed in these environments?’ is far from being resolved.⁶⁹ In cold molecular clouds such as in TMC-1 and in circumstellar envelopes of, for instance, IRC+10216, early chemical reaction models suggest that this radical is formed via a dissociative recombination of an electron from the cosmic radiation field with a diacetylene cation (equation (1)). However, these models underestimate the observed column densities of up to one order of magnitude.⁷⁰ In recent years, these reaction networks have been upgraded significantly, and various classes of reactions between two neutral particles, for instance of carbon atoms and ethynyl radicals with unsaturated hydrocarbons, have been incorporated.⁷¹ However, even these refined networks incorporating reactions (2) and (3) still fall short to explain the astronomically observed fractional abundances of the 1,3-butadiynyl radical by a factor of 2 – 3; note that the authors did not discriminate between the structural isomers of the C₃H₂ species.⁷² Although a preliminary crossed beam study of dicarbon molecules with acetylene suggested that both ground state ($X^1\Sigma_g^+$) and electronically excited ($a^3\Pi_u$) dicarbon can actually synthesize 1,3-butadiynyl, C₄H($X^2\Sigma^+$), radicals under single collision conditions via a hydrogen exchange pathway (equation (4)),⁷³ the reactions of dicarbon with unsaturated hydrocarbons and their hydrogen deficient radicals have neither been comprehensively incorporated into combustion nor interstellar reaction models.

This is actually very surprising since both the dicarbon molecule and the acetylene reactant are ubiquitous in cold molecular clouds,⁷⁴ circumstellar envelopes,⁷⁵ cometary comae,^{76,77,78} chemical vapor deposition processes,⁷⁹ and combustion flames.^{80,81,82} Here, the spectral lines of dicarbon in its $^1\Sigma_g^+$ electronic ground state were first detected in comets⁸³ and then in terrestrial hydrocarbon flames.⁸⁴ Note that in inner cometary coma of P/Halley at distances less than 10^4 km from the nucleus, also excited dicarbon molecules have been observed.⁷⁶ In the decades following it became clear that $C_2(X^1\Sigma_g^+)$ is ubiquitous in the interstellar medium⁸⁵ and in combustion flames.^{50,86} Transitions were observed towards warm carbons stars like IRC+10126,⁸⁷ post AGB stars such as HD 56126, and towards the HII region W40 IRS.⁸⁸ Note that in carbon stars, averaged translational temperatures of about 3000 – 3500 K of the dicarbon molecules have been derived.⁸⁷ Very recently, John et al. and Shiomi et al. suggested that dicarbon is the actual precursor in the formation of nanocrystalline diamond;^{89,90,91} number densities in $H_2/Ar/CH_4$ plasmas have been determined in the order of 10^{13} cm^{-3} . These processes are closely related to the growth of carbon clusters in carbon-rich stars⁹² as well as to the synthesis of diamonds in hydrogen-poor preplanetary nebulae⁹³ and in our solar system.⁹⁴ Also, it has been suggested that in combustion flames and chemical vapor deposition processes,⁹⁵ dicarbon molecules can be formed from acetylene with metastable bath molecules and atoms such as nitrogen and helium (equation (5)). Acetylene flames, for instance, produce an extremely bright source of dicarbon emission over the entire optical range. The translational and rotational temperatures in the flame are equal to each other with an average value of $1100 \pm 300\text{K}$. Secondary reactions in the flame produce several dense bands in the red which are likely due to soot-forming precursor molecules.^{96,97} In circumstellar envelopes and in interstellar clouds, dicarbon is likely to be produced via dissociative recombination of an electron with an acetylene cation (equation (6)), whereas in comets, ground and electronically excited dicarbon species are suggested to be generated easily via photolysis of the ethynyl radical (equation (7))^{98,99} or via multi photon dissociation of acetylene ($C_2H_2(X^1\Sigma_g^+)$).¹⁰⁰





Due to the importance of dicarbon molecules as potential precursors to PAHs and to their hydrogen deficient precursor molecules, the electronic states^{101,102,103,104,105} and the inherent kinetics of dicarbon reactions with various collision partners like alkanes^{106,107} and their unsaturated counterparts,¹⁰⁸ alcohols,¹⁰⁹ as well as molecular ions¹¹⁰ have been investigated. For instance, the disappearance of $\text{C}_2(\text{X}^1\Sigma_g^+, \text{a}^3\Pi_u)$ in the presence of an acetylene reactant gas was found to be very fast at 300 K with rate constants of $4.3 \times 10^{-10} \text{ cm}^3\text{s}^{-1}$ and $0.9 \times 10^{-10} \text{ cm}^3\text{s}^{-1}$ for the $\text{X}^1\Sigma_g^+$ and $\text{a}^3\Pi_u$ states, respectively; recall that the electronically excited triplet state, $\text{a}^3\Pi_u$, lies only 718.32 cm^{-1} (8.6 kJmol^{-1}) above the ground state $\text{X}^1\Sigma_g^+$.¹¹¹ However, although these studies provided valuable information on the reaction rates, neither the reaction products nor the intermediates involved could be identified. However, the latter are of paramount importance to the combustion modeling community. Due to this importance, we investigate the collision-energy dependent chemical dynamics of the reaction between dicarbon molecules in their $\text{X}^1\Sigma_g^+$ and $\text{a}^3\Pi_u$ electronic states with acetylene, $\text{C}_2\text{H}_2(\text{X}^1\Sigma_g^+)$, under single collision conditions at six collision energies between 10 kJ mol^{-1} and 50 kJmol^{-1} . The detailed information on the reaction dynamics also disclose the nature of the hitherto poorly explored singlet and triplet C_4H_2 potential energy surfaces (PESs),^{112,113,114} and the formation of C_4H isomer(s) in interstellar environments, chemical vapor deposition processes, and in hydrocarbon flames.

2. Experimental Setup and Data Processing

The experiments were conducted under single collision conditions in a crossed molecular beams machine at The University of Hawaii. The main chamber consists of a 304 stainless steel box ($180 \text{ cm} \times 160 \text{ cm} \times 80 \text{ cm}$; 2300 l) and is evacuated by three 2000 ls^{-1} magnetically suspended turbo molecular pumps (Osaka Vacuum; TG 2003) backed by a single scroll pump (Edwards XD35; 10 ls^{-1}) to the low 10^{-8} torr region (Figure 2). To reduce the background from straight-through molecules into the detector, the machine is also equipped with a cold shield located between the chopper wheel and the interaction region (primary source) and downstream the skimmer (secondary source). This oxygen free high conductivity (OFHC) copper shield is inter-

faced to the 10 K stage of a CTI CP-1020 cold head and improves the vacuum in the main chamber to 4×10^{-9} torr. This arrangement keeps the pressure in the main chamber during an actual experiment to about 5×10^{-7} torr. Two source chambers are located inside the main chamber; in its current geometry, both reactant beams cross perpendicularly. Each source chamber is pumped by a 2000 ls^{-1} and a 430 ls^{-1} maglev pump (Osaka Vacuum; TG2003 and TG430) to the medium 10^{-9} torr region; operating pulsed sources increase the pressure to about 10^{-5} torr. A dry roots pump (Leybold WS505; 140 ls^{-1}) roughed by two oil-free EcoDry M30 pumps (Leybold; 16 ls^{-1}) backs the turbo pumps of each source chamber.

Pulsed dicarbon beams with number densities of up to $3 \times 10^{13} \text{ cm}^{-3}$ reactant species in the interaction region were generated in the primary source via laser ablation of graphite at 266 nm (8 mJ - 40 mJ per pulse), Table 1. Here, the 30 Hz output of a Spectra Physics GCR 270-30 Nd-YAG was focused onto a rotating carbon rod.¹¹⁵ The ablated species (atomic carbon $\text{C}(^3\text{P}_j)$, dicarbon $\text{C}_2(\text{X}^1\Sigma_g^+/\text{a}^3\Pi_u)$, tricarbon $\text{C}_3(\text{X}^1\Sigma_g^+)$) were seeded in neat carrier gas (helium, 99.9999 %; neon, 99.9999 %; argon: 99.9999 %) released by a Proch-Trickl pulsed valve (1.0 mm nozzle diameter). The latter was operated at - 400 V with 60 Hz, 80 μs pulses, and 4 atm backing pressure. The ablation laser was typically fired 150 μs – 165 μs after the pulsed valve has been triggered. The seeded beam passed the skimmer of 1.0 mm diameter. A four-slot chopper wheel mounted 35 mm after the ablation zone selected a 18.0 μs segment of the pulse. This segment of the dicarbon beam crossed a pulsed acetylene beam (C_2H_2 ; 99.99 %) released by a second pulsed valve perpendicularly under a well-defined collision energy in the interaction region (- 500 V; 80 μs pulses; 550 torr backing pressure; 0.75 mm nozzle diameter; acetone traces in the acetylene were removed by passing the acetylene gas through a molecular sieve and then through a dry-ice acetone mixture) (Table 1). Since the dicarbon beam was actually faster than the acetylene beam, the pulsed valve of the secondary source had to be actually triggered 10 – 20 μs prior to the one in the primary source. The divergences of the primary and secondary beams were determined to be of 3.0° and 4.3° , respectively; self-attenuation of the supersonic beams due to nozzle - skimmer interferences was minimized by optimizing the nozzle - skimmer distance in the primary and secondary source to 21 mm and 18 mm, respectively. Note that although the primary beam also contains tricarbon molecules, the latter were found not to react with acetylene if the

collision energy is below $\approx 86 \text{ kJmol}^{-1}$.¹¹⁶ Likewise, the carbon atoms do not interfere with the reactive scattering signal of the dicarbon – acetylene reaction at mass-to-charge ratios of 49 (C_4H^+) and 48 (C_4^+) since the heaviest products of the carbon atom – acetylene reactions show signal at 37 (C_3H^+) and 36 (C_3^+).¹¹⁷

The reactively scattered species are monitored using a quadrupole mass spectrometric detector (QMS). Actually, the detector is located in a separate, triply differentially pumped ultra high vacuum chamber (10^{-11} torr) and is rotatable within the plane defined by both beams. Since every rotation in a vacuum system increases the pressure, the rotating detector ring is separated by three teflon loaded seals from the atmosphere. The spaces between these seals are doubly differentially pumped to reduce the pressure from atmosphere (760 torr) via 10^{-2} torr and 4×10^{-8} torr (teflon sealed regions) to 4×10^{-9} torr in the main chamber. This arrangement ensures no pressure increase in the main chamber even if the detector is being rotated. Differentially pumped detector regions I/II reduce the gas load from the main chamber, whereas region III contains the Brink-type electron impact ionizer¹¹⁸ surrounded by a liquid nitrogen cold shield. The quadrupole mass filter and the Daly-type scintillation particle detector¹¹⁹ are connected to the second region. Note that each region is pumped by a magnetically levitated turbo molecular pump (region I/II: 400 ls^{-1} ; region III: 380 ls^{-1}); all three pumps are backed by a 400 ls^{-1} turbo molecular pump whose exhaust is connected to an oil free scroll pump (10 ls^{-1}). This pumping scheme reaches down to the low 10^{-11} torr in region three; lower pressures down to the high 10^{-13} torr regime can be achieved by operating a cold head inside region three (4 K; 1.5 W). In the present experiment, we focus on the detection of the C_4H^+ ($m/e = 49$) and C_4^+ ($m/e = 48$) ions. These masses are essentially background free; small background counts (about 0.5 counts per channel per 1024 TOF) arise from $^{191}\text{Ir}^{4+}$ ($m/e = 47.8$) and $^{193}\text{Ir}^{4+}$ ($m/e = 48.6$). These multiple charged ions originate from the filament of the ionizer (see below) and cannot be eliminated by operating the cold head in the ionizer region.

Recall that the actual ionizer consists of a thoriated iridium filament spot welded to a gold plated stainless steel cylindrical can, a meshed wire grid, and an extractor lens held at -150 V. We incorporated a four lead circuit, i.e. feeding two instead of one wire to the anode and cathode of the filament, respectively. This circuit eliminates the resistance of the leads to the filament and

hence diminishes voltage drops. The reduced voltage drop in turn minimizes the heat released from the filament to typically 6.6 W (1.9 V and 3.5 A for 2 mA emission current from a thoriated iridium filament). The electron energy, i.e. the potential difference between the can and the grid, was held at 200 eV, whereas the ion energy was kept at +36 eV. The extracted ions pass the entrance lens of the quadrupole rods (- 140 V), are separated in the quadrupole system, leave the exit lens (- 140 V), and are accelerated towards an aluminum coated stainless steel target maintained at -25 kV. The quadrupole mass filter and the Daly-type scintillation particle detector are connected to region II. Here, each ion hits the surface of a high voltage target (- 25 kV) and initiates an electron cascade. The latter is accelerated to an aluminum coated (200 nm) organic scintillator BC-418 (Saint Gobain; 391 nm photon emission) whose photon cascade is detected by a convection cooled photomultiplier tube (PMT; Burle 8850; 1100 - 1350 V) mounted outside the UHV detector. Magnetic shielding of the PMT and the resistor chain enhances the signal by about 15 %. Each PMT pulse passes then a discriminator set between 1.5 and 2.0 mV and is amplified. The outgoing TTL pulse is fed into a multi channel scaler (MCS) operated at dwell times between 0.64 μ s (on axis beam diagnostics) and 5.12 μ s or 10.24 μ s (reactive scattering experiments) to record the flight time of the ion versus the intensities at a defined mass-to-charge ratio (m/e) (TOF mode). These TOF spectra can be taken at distinct mass-to-charge ratios (m/e) and at different laboratory angles. By taking and integrating the TOF spectra at distinct laboratory angles in 2.5° steps, we can also obtain the laboratory angular distribution, i.e. the integrated signal intensity of an ion of distinct m/e versus the laboratory angle. For each angle, we accumulated up to 1.5×10^6 (argon seeding), 6.0×10^5 (neon seeding), and 3.0×10^5 (helium seeding) TOF spectra, averaged over several angular scans. The velocity of the supersonic dicarbon beam was monitored frequently after taking the data for five angles. Reference angles were chosen at the corresponding center-of-mass angles (Table 1) to calibrate fluctuating dicarbon beam intensities.

Information on the chemical dynamics of the reaction was obtained by fitting these TOF spectra of the reactively scattered products and the product angular distribution in the laboratory frame (LAB) using a forward-convolution routine. This procedure initially assumes an angular distribution $T(\theta)$ and a translational energy distribution $P(E_T)$ in the center-of-mass reference frame (CM). Due to the complex dynamics involved, the $P(E_T)$ is chosen in point form, whereas

the $T(\theta)$ is defined as a sum of three Legendre polynomials $P_l(\cos \theta)$ with the weighting coefficients a_l (equation (8)). Laboratory TOF spectra and the laboratory angular distribution were then calculated from these $T(\theta)$ and $P(E_T)$ accounting for the transformation Jacobian and averaging over the apparatus (chopper frequency; detector opening) and beam functions (velocity spread, angular spread). Best fits of the TOF and laboratory angular distributions were achieved by refining the adjustable $T(\theta)$ parameters and the points of the $P(E_T)$. The final outcome is the generation of a product flux contour map which reports the differential cross section, $I(\theta, u)$, of the product as the intensity as a function of angle θ and product center-of-mass velocity u (equation (9)). This map serves as an image of the reaction and contains all the information of the reactive scattering process.

$$(8) \quad T(\theta) = \sum_{l=0}^2 a_l \times P_l(\cos \theta)$$

$$(9) \quad I(\theta, u) \sim P(u) \times T(\theta).$$

Table 1: Peak velocities (v_p), speed ratios (S), center-of-mass angles (Θ_{CM}), together with the nominal collision energies of the dicarbon and the acetylene reactants (E_c).

beam	v_p (ms ⁻¹)	S	E_c , kJmol ⁻¹	Θ_{CM}
$C_2(X^1\Sigma_g^+/a^3\Pi_u)/Ar$	944 ± 8	5.0 ± 0.1	10.6 ± 0.1	46.0 ± 0.3
$C_2(X^1\Sigma_g^+/a^3\Pi_u)/Ne$	1060 ± 17	4.7 ± 0.5	12.1 ± 0.2	42.7 ± 0.5
$C_2(X^1\Sigma_g^+/a^3\Pi_u)/He$	1629 ± 6	5.2 ± 0.1	21.6 ± 0.2	31.0 ± 0.2
$C_2(X^1\Sigma_g^+/a^3\Pi_u)/He$	1956 ± 23	5.7 ± 0.2	29.0 ± 0.5	26.5 ± 0.2
$C_2(X^1\Sigma_g^+/a^3\Pi_u)/He$	2362 ± 42	4.9 ± 0.3	39.9 ± 0.2	22.5 ± 0.4
$C_2(X^1\Sigma_g^+/a^3\Pi_u)/He$	2608 ± 36	4.1 ± 0.2	47.5 ± 1.2	20.5 ± 0.2
$C_2H_2(X^1\Sigma_g^+)$	902 ± 2	16.0 ± 1.0	-	-

3. Electronic Structure Calculations

Most details of the potential energy surfaces for the dicarbon ($C_2(X^1\Sigma_g^+)/C_2(a^3\Pi)$) plus acetylene ($C_2H_2(X^1\Sigma_g^+)$) reactions were described in our previous publication.⁷³ Here, we additionally consider the possibility of molecular hydrogen elimination from the C_4H_2 intermediates in the singlet and triplet states to produce also tetracarbon C_4 in its electronic ground ($X^3\Sigma_g^-$) and/or first excited states ($a^1\Sigma_g^+$). Finally, we investigated direct abstraction pathways of a hydrogen atom by a dicarbon molecule to form the ethynyl radical ($C_2H(X^2\Sigma^+)$). Geometries of various intermediates, transition states, and products involved in these channels have been optimized using the hybrid density functional B3LYP/6-311G(d,p) level of theory.¹²⁰ Vibrational frequencies have been computed using the same theoretical method; relative energies have been refined by single-point restricted coupled cluster RCCSD(T)/6-311+G(3df,2p) calculations.¹²¹ The ab initio GAUSSIAN 98¹²² and MOLPRO 2002¹²³ program packages were utilized.

4. Results

4.1. Reactive Scattering Signal

We observed signal at mass-to-charge ratios of $m/e = 49$ (C_4H^+), $48(C_4^+)$, 37 (C_3H^+), and 36 (C_3^+). At all laboratory angles, the TOF spectra at $m/e = 49$ (C_4H^+) (Figures 3-4), $48(C_4^+)$, and 37 (C_3H^+) depict identical patterns and could be fit at each collision energy with identical center-of-mass functions. Therefore, the signal at $m/e = 48$ and 37 originates in cracking of the C_4H^+ parent in the ionizer. However, the TOFs taken at $m/e = 36$ differ strongly from the higher masses.¹¹⁷ Here, the signal arises from two contributions: first, fragmentation of the C_4H^+ parent in the ionizer to C_3^+ (slow part) and secondly from the $C_3(X^1\Sigma_g^+) + H_2(X^1\Sigma_g^+)$ channel (fast part) which is open in the reaction of atomic carbon, $C(^3P_j)$ with acetylene.^{116,124} Recall that the Newton circles of the linear and cyclic C_3H isomers, which are also formed in bimolecular collisions of atomic carbon with acetylene, do not overlap with those of the 1,3-butadiynyl radical. Therefore, neither C_3H isomer can be detected at those angles at which 1,3-butadiynyl can be monitored, and signal at $m/e = 37$ solely originates from fragmentation of the C_4H^+ parent in the ionizer. Note that no radiative association of dicarbon and acetylene to yield C_4H_2 ($m/e = 50$) was detected; we monitored a small signal at $m/e = 50$, but the intensity of about 4-5 % of the

C_4H^+ signal at $m/e = 49$ and the TOF shape, which is identical to $m/e = 49$, suggest that this signal originates from the $^{13}CC_3H^+$ isotopomer.

4.2. Laboratory Angular Distributions (LAB) and TOF spectra

The most probable Newton diagrams of the reactions of dicarbon $C_2(X^1\Sigma_g^+/a^3\Pi_u)$ with acetylene to form 1,3-butadiynyl ($C_4H(X^2\Sigma^+)$) plus atomic hydrogen ($H^2S_{1/2}$) and the laboratory angular distributions of the heavy C_4H product recorded at $m/e = 49$ are displayed in Figure 3(a)-(f) for six collision energies. The corresponding TOF spectra are presented in Figures 4(a)-(f). The LAB distributions are relatively narrow and spread at least over 32° in the scattering plane ($E_c = 47.5 \pm 1.2 \text{ kJmol}^{-1}$). As expected from the kinematics of the reaction (constant exoergicity and velocity of the acetylene beam, but changing velocity vector of the dicarbon beam), the angular spread of the scattering signal increases by about 10° to 42° at the lowest collision energy of $10.6 \pm 0.1 \text{ kJmol}^{-1}$. The relatively small angular spreads suggest that a comparatively small fraction of the total available energy is released as translational energy of the 1,3-butadiynyl and atomic hydrogen products. This is also reflected in the relatively small width of the TOF spectra of only 250 - 350 μs . It is worth mentioning that at lower collision energies of $10.6 \pm 0.1 \text{ kJmol}^{-1}$, $12.1 \pm 0.2 \text{ kJmol}^{-1}$, and $21.6 \pm 0.2 \text{ kJmol}^{-1}$, the LAB distribution is forward scattered with respect to the dicarbon beam. As the collision energies increase, the LAB distributions become less forward scattered. As a matter of fact, a pronounced switching from a forward-scattered to backward scattered distribution can be observed at a collision energy of $29.0 \pm 0.5 \text{ kJmol}^{-1}$. The trend actually amplifies by rising the collision energy even higher via $39.9 \pm 0.2 \text{ kJmol}^{-1}$ to $47.5 \pm 1.2 \text{ kJmol}^{-1}$.

4.3. Center-of-Mass Translational Energy Distributions, $P(E_T)$ s

Figure 5 presents the translational energy distributions in the center-of-mass-frame, $P(E_T)$, together with the center-of-mass angular distributions, $T(\theta)$. Best fits of the TOF spectra and the LAB distributions were achieved at each collision energy with a single $P(E_T)$ extending to a maximum translational energy, E_{max} , of 47 kJmol^{-1} ($E_c = 10.6 \text{ kJmol}^{-1}$), 50 kJmol^{-1} ($E_c = 12.1 \text{ kJmol}^{-1}$), 60 kJmol^{-1} ($E_c = 21.6 \text{ kJmol}^{-1}$), 70 kJmol^{-1} ($E_c = 29.0 \text{ kJmol}^{-1}$), 80 kJmol^{-1} ($E_c = 39.9 \text{ kJmol}^{-1}$),

and 90 kJmol^{-1} ($E_c = 47.5 \text{ kJmol}^{-1}$). Due to the kinematics of the reaction, i.e. an emission of a light hydrogen atom, the fits are relatively insensitive to the high energy cut-off: adding or cutting the high energy tail by $\pm 5 \text{ kJmol}^{-1}$ did not influence the quality of the fit. Since the maximum translational energy presents simply the sum of the collision energy and the absolute of the exoergicity of the reaction, the magnitude of E_{max} can be utilized to compute the reaction exoergicity. Averaging over six collision energies, we determine that the $\text{C}_4\text{H}(\text{X}^2\Sigma^+) + \text{H}(^2\text{S}_{1/2})$ channel is exoergic by $39.9 \pm 5.0 \text{ kJmol}^{-1}$. We can analyze the center-of-mass translational energy distributions even further. Recall that the most probable translational energy gives the order-of-magnitude of the barrier height in the exit channel. All $P(E_T)$ s depict a flat and very broad plateau between $3 - 17 \text{ kJmol}^{-1}$; the latter presents an upper limit at the highest collision energy investigated in this study. These data suggest that at least one reaction channel exhibits an exit barrier and, hence, a significant geometry as well as electron density change from the fragmenting C_4H_2 intermediate to the products resulting in a repulsive bond rupture from a tight transition state. Also, the peaking of the $P(E_T)$ at lower collision energies close to zero translation energy could indicate the existence of a second reaction pathway which involves almost no exit barrier and hence a loose exit transition state. Note that the presence of an exit barrier is further indicated by the fraction of energy released into translational motion of the products (Figure 6). From the center-of-mass translational energy distributions, we can compute the averaged translation energy, $\langle E_T \rangle$, and plot the later versus the nominal collision energy, E_c . As the collision energy increases, the averaged translational energy rises, too. A linear relationship between $\langle E_T \rangle$ and E_c was derived to be equation (10). Also, the fraction of the energy channeling into the translational modes of the products, $\langle E_T \rangle / E_{\text{max}}$, can be plotted versus the collision energy. Here, a slight increase from about $31 \pm 2 \%$ to $34 \pm 2 \%$ from the lowest to the highest collision energy can be seen. These data can also be fit with a linear relationship, equation (11).

$$(10) \quad \langle E_T \rangle = (0.37 \pm 0.02) \times E_c + (13.3 \pm 0.4).$$

$$(11) \quad \langle E_T \rangle / E_{\text{max}} = (5.5 \pm 0.6) \times 10^{-5} \times E_c + (0.35 \pm 0.02).$$

4.4. Center-of-Mass Angular Distributions, $T(\theta)$ s

Based on LAB distributions (Figure 3), the trend of the collision-energy dependence of the center-of-mass angular distributions, $T(\theta)$ s (Figure 5), can be foreseen. As the collision energy increase, the shapes of the $T(\theta)$ s changes dramatically. The center-of-mass angular distributions vary from a forward scattered distribution with an intensity ratio of $T(\theta)$ at $\theta = 0^\circ$ to 180° of $T(0^\circ)/T(180^\circ) = 2.0 \pm 0.3$ at the lowest collision energy of 10.6 kJmol^{-1} to a backward scattered distribution with $T(0^\circ)/T(180^\circ) = 0.5 \pm 0.1$ at the highest collision energy of 47.5 kJmol^{-1} . At both lower collision energies of 10.6 kJmol^{-1} and 12.1 kJmol^{-1} , the distributions were found to be mildly sideways peaked at about $30^\circ \pm 10^\circ$ and $55^\circ \pm 5^\circ$. Note that at intermediate collision energies of 21.6 kJmol^{-1} and 29.0 kJmol^{-1} , the $T(\theta)$ s are relatively weakly polarized. Figure 7 summarizes the collision energy dependence of the ratios of the center-of-mass angular distributions at the poles. The data could be fit with a decaying exponential function (equation (12)).

$$(12) \quad T(0^\circ)/T(180^\circ) = (0.41 \pm 0.09) \times (3.53 \pm 0.34) e^{-(E_c/(13.5 \pm 2.2))}.$$

Here, the energy dependent shapes of the center-of-mass angular distributions do not propose the existence of a conventional osculating C_4H_2 complex.¹²⁵ The results rather suggest two microchannels. These are (1) an isotropic channel possibly symmetric around $\theta = \pi/2$ governed by indirect scattering dynamics and by a weak coupling between the initial and final orbital angular momenta \mathbf{L} and \mathbf{L}' perpendicular to the initial and final relative velocity vectors \mathbf{v} and \mathbf{v}' (microchannel 1) and (2) a strongly impact parameter dependent microchannel (forward scattered at lower and backward scattered at higher collision energies) with a strong correlation of \mathbf{L} and \mathbf{L}' (microchannel 2).

Two scenarios might account for a potential forward-backward symmetry of the center-of-mass angular distribution of microchannel 1. First, the fragmenting C_4H_2 intermediate resides in a deep potential energy well and has a lifetime τ longer than its rotational period. Secondly, a decomposing symmetric intermediate can result in a center-of-mass angular distribution symmetric around $\pi/2$ despite a complex lifetime shorter than its rotational period since the hydrogen atom from either end could depart with equal probability in θ and $\pi-\theta$. Here, the departing atoms would be inter convertible by a rotational axis.¹²⁴ Since the intermediate has a generic formula C_4H_2 , this restricts the consideration to a C_2 axis which must prevail in the decomposing

complex; therefore, the fragmenting intermediate must belong to the C_2 , D_2 , C_{2v} , C_{2h} , or $D_{\infty h}$ point group. The weak polarization of this microchannel can be understood in terms of total angular momentum conservation and angular momentum disposal. Neglecting the nuclear momenta of the protons, the total angular momentum \mathbf{J} is given by equation (13) with the rotational angular momenta of the reactants and products \mathbf{j} and \mathbf{j}' . A significant simplification is introduced by comparing the magnitude of \mathbf{L} and \mathbf{j} . Since bulk experiments indicate that the reaction of dicarbon molecules with acetylene proceeds within gas kinetics and orbiting limits,¹¹¹ the maximum impact parameter b_{\max} leading to an initial complex formation can be approximated in terms of the classical capture theory.¹²⁶ This treatment suggests maximum impact parameters between $b_{\max}(10.6 \text{ kJmol}^{-1}) = 6.8 \text{ \AA}$ and $b_{\max}(47.5 \text{ kJmol}^{-1}) = 5.4 \text{ \AA}$ for the reaction of ground state dicarbon molecules with acetylene. The maximum orbital angular momentum L_{\max} relates to b_{\max} via equation (14) where μ is the reduced mass of the reactants and v_r the relative velocity of both reactants. This brings us to a maximum orbital angular momentum of between $L_{\max}(10.6 \text{ kJmol}^{-1}) = 173 \hbar$ and $L_{\max}(47.5 \text{ kJmol}^{-1}) = 283 \hbar$. Since acetylene is prepared in a supersonic expansion and j peaks at only $3\text{-}5 \hbar$ at a typical rotational temperature of $20 \text{ K} - 30 \text{ K}$, \mathbf{j} contributes less than 3% to the total angular momentum. Therefore, \mathbf{J} becomes the initial orbital angular momentum \mathbf{L} , and equation (13) can be rewritten as equation (15). At medium collision energies of 21.6 kJmol^{-1} and 29.0 kJmol^{-1} , the experimentally observed weak coupling between \mathbf{L} and \mathbf{L}' suggests that on average L' is much smaller than L ; similar systems studied suggest that L' is in the order of $0.1 - 0.2 L$. Since equation (14) can be rewritten as equation (16) with L' the final orbital angular momentum, μ' the reduced mass of the products, and b' the exit impact parameter, we can see directly that the small reduced mass of the reaction products of $9.8 \times 10^{-4} \text{ kg mol}^{-1}$, i.e. about the mass of a hydrogen atom, translates into a small final orbital angular momentum L' . In other words, the weak $\mathbf{L}\text{-}\mathbf{L}'$ correlation is a direct result of large reactive impact parameters contributing to the complex formation and the inability of the departing hydrogen atom to carry away significant orbital angular momentum. The mildly sideways peaking of the angular distributions at both lower collision energies deserves particular attention. Here, the $T(\theta)$ peak mildly on a broad plateau between 40° and 60° resulting in a mildly sideways peaking, possibly suggesting that a minor fraction of the C_4H_2 complexes loses the hydrogen atom perpendicularly to the plane of the rotating intermediate and parallel to the total angular momentum vector \mathbf{J} . However, at higher collision energies, these geometrical constraints

are not pronounced. This means that if we consider the reversed reaction of a hydrogen atom adding to the 1,3-butadiynyl radical, higher collision energies allow a wider range of impact parameters to react.

$$(13) \quad \mathbf{J} = \mathbf{L} + \mathbf{j} = \mathbf{L}' + \mathbf{j}'$$

$$(14) \quad L_{\max} = \mu \times b_{\max} \times v_r.$$

$$(15) \quad \mathbf{L} \approx \mathbf{J} = \mathbf{L}' + \mathbf{j}'.$$

$$(16) \quad L' = \mu' \times b' \times v_r'.$$

4.5. Flux Contour Maps, I(u,q)s

The center-of-mass flux contour maps of the heavy reaction product (equation (9)) for all six collision energies are shown in Figure 8. As anticipated from the collision energy dependent shapes of the $T(\theta)$ s, the product fluxes peak in forward directions with respect to the dicarbon beam on the relative velocity vectors at lower collision energies and switch then to a backward-peaking as the collision energy rises. Also, at lower collision energies, the mildly sideways peaking is evident.

5. Discussion

5.1. Energetical Considerations

In case of polyatomic reactions, it is often useful to combine the reactive scattering experiments with electronic structure calculations of the potential energy surfaces involved (Figure 9). By comparing the conclusions from the center-of-mass translational energy ($P(E_T)$) and angular distributions ($T(\theta)$) with the theoretical investigation, a complete picture of the underlying reaction dynamics on the ground state singlet and excited state triplet surfaces emerges. Most importantly, we have determined that the formation of the C_4H isomer plus atomic hydrogen is – averaged over six collision energies - exoergic by $39.9 \pm 5.0 \text{ kJmol}^{-1}$. This value is in excellent agreement with the theoretically obtained energy of -40.4 kJmol^{-1} of the reaction of electronically excited dicarbon in its first excited triplet state, $C_2(a^3\Pi_u)$, with acetylene to form ground state 1,3-butadiynyl, $C_4H(X^2\Sigma^+)$, plus a hydrogen atom. Note that the energetics of ground state

dicarbon, $C_2(X^1\Sigma_g^+)$, reacting with acetylene are computed to be less favorable by about 7 kJ mol⁻¹; therefore, the experimentally determined energetics of the reactions of ground state and excited state dicarbon molecules with acetylene to form ground state 1,3-butadiynyl plus a hydrogen atom are in line with the computed values. Note that the five C_4H isomers p2 – p6 are less stable by 118.0, 140.2, 171.4, 74.8, and 230.6 kJmol⁻¹, respectively, compared to 1,3-butadiynyl radical (Figure 1). An earlier study of the C_4H isomers suggested another C_{2v} symmetric cyclic isomer, HC=c-C₃, to exist about 165 kJmol⁻¹ above p1.¹²⁷ However, we found that HC=c-C₃ actually has one imaginary frequency; once the C_{2v} symmetry is released, it optimizes to p1. Takahashi's study also yielded incorrect ground state of p1 and did not locate p3 and p4 as local minima. Considering the energetics of our calculations (Figure 1), the reaction energies to form p2 – p6 are calculated to be + 77.6, + 99.8, + 131.0, + 34.4 and + 190.2 kJmol⁻¹ on the triplet surface. Since the highest collision energy in our experiment was 47.5 kJmol⁻¹, these C_4H isomers are energetically not accessible, except p5 at the two highest collision energies. Therefore, we can conclude that the 1,3-butadiynyl radical is the sole C_4H structural isomer formed in the reaction of dicarbon with acetylene on the triplet surfaces at collision energies of 10.6, 12.1, 21.6, and 29.0 kJmol⁻¹. On the singlet surface, we can exclude p5 at all collision energies except 47.5 kJmol⁻¹. Since, however, the collision energy dependence of the averaged translational energy (Figure 6), of the fraction of the averaged translational energy (Figure 6), and of the ratio of the center-of-mass angular distribution at the poles (Figure 7) at both higher collision energies can be fit with the identical functions as at the lower collision energies (equations (10)-(12)), we can likely rule out the involvement of p5 at higher collision energies. This would be in line with the energetics of decomposition of the intermediates favoring the formation of the 1,3-butadiynyl radical.

We would like to address briefly the possibility of the formation of the 1,3-butadiynyl radical in its first excited $^2\Pi$ state which lies only 5.6 kJmol⁻¹ above the ground state; our theoretical value underestimated the experimentally determined singlet – triplet splitting by 3 kJmol⁻¹. Here, the processes to form $C_4H(A^2\Pi) + H(^2S_{1/2})$ via the reactions $C_2(X^1\Sigma_g^+) + C_4H_2(X^1\Sigma_g^+)$ and $C_2(a^3\Pi) + C_4H_2(X^1\Sigma_g^+)$ are exoergic by 27.7 kJmol⁻¹, and 34.8 kJmol⁻¹, respectively. Therefore, based on the energetics alone, we cannot exclude that minor contributions of $C_4H(A^2\Pi)$ is synthesized, and a closer look at the involved dynamics is necessary.

5.2. The Reaction Dynamics

5.2.1. Micro channel 1

Having identified the 1,3-butadiynyl radical as the sole C_4H product in the reaction of dicarbon with acetylene on the singlet and triplet surfaces, we attempt now to solve the underlying reaction dynamics. Based on the energy dependence of the center-of-mass functions and the theoretical calculations, the dynamics involve two microchannels, one reaction pathway on the singlet surface (micro channel 1) and a second pathway on the triplet surface (micro channel 2) (section 4). The isotropic micro channel 1 (section 4.4) suggests that the reaction proceeds via formation of C_4H_2 complex(es) and hence is indirect (complex forming reaction dynamics). Our computations show that the dicarbon molecule $C_2(X^1\Sigma_g^+)$ can add barrierlessly to the carbon-carbon triple bond forming the relatively weakly bound ($-288.1 \text{ kJmol}^{-1}$) 1-cyclopropene-1-methylidene structure (s-INT1). The latter isomerizes to the 1-cyclobuten-2-yne molecule (s-INT2). Alternatively, dicarbon can add in one step across the carbon-carbon triple bond to the acetylene molecule forming s-INT2 from the reactants without an entrance barrier. The s-INT2 intermediate undergoes ring opening to diacetylene (s-INT3) which resides in a deep potential energy well of 577.1 kJmol^{-1} compared to the separated reactants. All the involved isomerization barriers s-INT1 \rightarrow s-INT2 and s-INT2 \rightarrow s-INT3 are well below the energy of the dicarbon plus acetylene reactants. Note that this reaction sequence de-facto ‘inserts’ the dicarbon molecule via a three-step reaction pathway through an initial addition and two ring-isomerization processes into an extremely stable carbon-carbon triple bond of the acetylene molecule, i.e. a strong bond with a bond energy of 965 kJmol^{-1} . However, according to intrinsic reaction coordinate calculations for the transition state separating s-INT2 and s-INT3, this process is more complicated; one of the carbon atoms of the dicarbon indeed formally inserts between two acetylenic carbon atoms, while the second takes the terminal position in the C_4 chain and this is followed by a spontaneous hydrogen shift to this terminal carbon. So, if $C_2(X^1\Sigma_g^+)$ attacked per- ^{13}C labeled acetylene, $^{13}C_2H_2(X^1\Sigma_g^+)$, s-INT3 produced in this reaction should be $H^{13}CC^{13}CCH$. The diacetylene molecule can decompose then via a loose exit transition state in a barrier-less reaction to form $C_4H(X^2\Sigma^+) + H(^2S_{1/2})$ by hydrogen emission within the rotational plane of the complex through a simple bond rupture. The reversed reaction of a hydrogen atom with the 1,3-butadiynyl radical presents a prototype atom-radical recombination reaction without entrance

barrier. The loose exit transition state is also reflected in a merely mild geometry change from the diacetylene intermediate to the 1,3-butadiynyl radical from $r(\text{H-C1}) = 109.4$ pm, $r(\text{C1-C2}) = 121.8$ pm, and $r(\text{C2-C3}) = 138.3$ pm (diacetylene)¹²⁸ to $r(\text{H-C1}) = 106.3$ pm, $r(\text{C1-C2}) = 120.6$ pm, $r(\text{C2-C3}) = 136.5$ pm, and $r(\text{C3-C4}) = 121.1$ pm (1,3-butadiynyl). In a hypothetical crossed beams experiment of $\text{C}_2(\text{X}^1\Sigma_g^+)$ with per- ^{13}C labeled acetylene, $^{13}\text{C}_2\text{H}_2(\text{X}^1\Sigma_g^+)$, this reaction would yield $\text{H}^3\text{CC}^{13}\text{CC}(\text{X}^2\Sigma^+)$ or $^{13}\text{CC}^{13}\text{CCH} + \text{H}(\text{}^2\text{S}_{1/2})$. The barrier-less nature of the exit transition state was indicated in those parts of the center-of-mass translational energy distributions peaking close to zero translational energy (section 4.3). The deep potential energy well, in which s-INT3 resides, could result in the forward-backward symmetry of the center-of-mass angular distribution of micro channel 1 at lower collision energies due to the life time of diacetylene longer than its rotational period. Recall, however, that the diacetylene molecule belongs to the $\text{D}_{\infty\text{h}}$ point group. Since angular momentum conservation dictates that s-INT3 is excited to B like rotations around a C_2 symmetry axis, this intermediate must be classified as ‘symmetric’. In other words, the linear diacetylene molecule can lose a hydrogen atom from either acetylenic end scattering it with equal probability into θ and $\pi-\theta$. Therefore, even if the lifetime of the diacetylene intermediate is actually shorter than its rotational period, the symmetry produces center-of-mass angular distributions symmetric around $\pi/2$ (section 4.4). This would explain the collision-energy invariant isotropic shape of the center-of-mass angular distribution. A similar behavior has been observed in the $\text{C}(\text{}^3\text{P}_j) + \text{C}_2\text{H}_2(\text{X}^1\Sigma_g^+)$ reaction.¹²⁴ Here, a C_2 symmetric triplet propargylene intermediate ($\text{HCCCH}(\text{X}^3\text{B})$) was found to produce an isotropic center-of-mass angular distribution at collision energies between 8.8 kJmol^{-1} and 45.0 kJmol^{-1} . This barrier-less, indirect, and exoergic reaction pathway can also account for the fast rate constants of this reaction (4.3×10^{-10} cm^3s^{-1}) measured under bulk conditions at 300 K.¹⁰⁸

Before we switch to the triplet surface, it is worth discussing the symmetry of the reactive surface. The $^1\Sigma_g^+$ ground state of the diacetylene molecule correlates with both ground state $\text{C}_4\text{H}(\text{X}^2\Sigma^+) + \text{H}(\text{}^2\text{S}_{1/2})$ reaction products. As a matter of fact, the point groups of s-INT2 and of the transition states involved in the s-INT1 \rightarrow s-INT2 and s-INT2 \rightarrow s-INT3 rearrangements dictate that C_2 presents the highest feasible symmetry under which this reaction can proceed until the formation of the diacetylene intermediate. However, the 1,3-butadiynyl reaction product be-

longs to the $C_{\infty v}$ point group and hence loses its C_2 symmetry axis parallel to the principal rotational axis. This reduces the point group and the symmetry of the total electronic wave functions of reactants, involved intermediates, and products to C_1 and 1A , respectively. We can also utilize angular momentum conservation to show that the reaction must proceed on the 1A surface, i.e. without any symmetry element. Here, both the diacetylene reaction intermediate (s-INT3) as well as the 1,3-butadiynyl radical must be excited to B-like rotations. Since angular momentum must be conserved even during the isomerization process $s\text{-INT2} \rightarrow s\text{-INT3}$, s-INT2 rotates around the B/C axis. A rotation around the A axis is not feasible; here, the ring opening from s-INT2 to s-INT3 would translate into rotations of the linear diacetylene molecule around the molecular axis; these rotational excitations are, however, energetically not accessible. Let us have now a closer look at the isomerization pathway from s-INT1 to s-INT2. Since s-INT2 can rotate only around its B/C axis, angular momentum conservation suggests that s-INT1 also should be excited to these rotations. Rotations around the A principal axis of s-INT1 can be eliminated since an s-INT1 excited to A-like rotations would result after crossing the isomerization barrier into s-INT2 intermediates rotating around the A axis; however, the latter have been already eliminated from the discussion. Summarized, angular momentum conservation suggests that the following rotations can be only excited: s-INT1: B/C, s-INT2: B/C, s-INT3: B, p1: B. These rotations have no common symmetry element, and the reaction must proceed under C_1 symmetry, hence on the 1A surface.

Finally, we would like to discuss the potential involvement of two reaction intermediates s-INT4 and s-INT5. A hydrogen migration in s-INT1 can lead to s-INT4; the latter can undergo ring opening to yield butatrienylidenecarbene (s-INT5). All barriers involved in these isomerization steps range below the total energy of the separated reactants. Based on our calculations, s-INT5 can decompose either via atomic hydrogen loss to form $C_4H(X^2\Sigma^+) + H(^2S_{1/2})$ or through molecular hydrogen loss to yield electronically excited tetracarbon, $C_4(a^1\Sigma_g^+) + H_2(X^1\Sigma_g^+)$ in an endoergic reaction (+ 34.9 kJmol⁻¹). Based on the energetics alone, we should have observed molecular hydrogen at those experiments carried out at collision energies of 39.9 kJmol⁻¹ and 47.5 kJmol⁻¹. However, our data clearly showed no sign of a molecular hydrogen loss. How can this apparent discrepancy be explained? In principle, the $C_4(a^1\Sigma_g^+) + H_2(X^1\Sigma_g^+)$ products can be formed from the intermediates s-INT3 and s-INT5. However, a careful search of

a transition state for molecular hydrogen elimination from diacetylene (s-INT3) showed that no first-order saddle point exists on this pathway. The energies of possible transition state candidates for such 1,4-H₂ elimination are very high and transition state optimization converges to the separated C₄(a¹Σ_g⁺) + H₂(X¹Σ_g⁺) products. On the other hand, H₂(X¹Σ_g⁺) loss from s-INT5 takes place without an exit barrier. In order to prove this, calculations of the minimal energy reaction path (MEP) from C₄(a¹Σ_g⁺) + H₂(X¹Σ_g⁺) to s-INT5 were performed by scanning PES keeping the distance from a terminal carbon atom of tetracarbon to the center of the H-H bond frozen at different values from 4.0 Å to 1.0 Å and optimizing all other geometric parameters. These calculations showed that the energy of the system steadily decreases when H₂(X¹Σ_g⁺) approaches the terminal carbon atom of C₄(a¹Σ_g⁺), with barrierless formation of two new C-H bonds and cleavage of the H-H bond. Thus, just like in the reaction of CH₂(a¹A₁) + H₂(X¹Σ_g⁺) to form methane, the lone pair of the carbon atom inserts into the H-H bond of molecular hydrogen without a barrier. The s-INT5 → C₄(a¹Σ_g⁺) + H₂(X¹Σ_g⁺) reaction step is computed to be highly endothermic, by 429 kJmol⁻¹, but it occurs without a distinct transition state and exit barrier. Since we did not observe any molecular hydrogen elimination channel, this suggests that the formation of the s-INT5 intermediate must be hindered. Let us have a closer look at the formation process of s-INT5. Actually, s-INT1 presents the crucial collision complex which can either isomerize to s-INT2 or to s-INT4. Considering the relative barrier heights of 65.4 kJmol⁻¹ and 224.1 kJmol⁻¹, respectively, it is obvious that the s-INT1 → s-INT2 pathway should dominate over the s-INT1 → s-INT4 route. This conclusion is supported by RRKM calculations. The ratio of both rate constants varies from 4.3 × 10⁴ to 4.2 × 10³ at collision energies of 0 kJmol⁻¹ and 50 kJmol⁻¹. Thus the channel via s-INT2 is at least three orders of magnitude faster than that via s-INT4, and the latter can be safely ruled out. Therefore, both the experiments and electronic structure calculations agree that – at least on the singlet surface – molecular hydrogen should not be formed.

5.2.2. Micro channel 2

We identified the 1,3-butadiynyl radical, C₄H(X²Σ⁺), plus a hydrogen atom as the sole reaction products on the triplet surface (sections 4.1. & 5.1.). What is the actual formation pathway to form the 1,3-butadiynyl radical? Our computations suggest that three entrance channels

exist on the triplet C_4H_2 surface; all pathways have no entrance barrier and proceed via addition of the dicarbon molecule to the carbon-carbon triple bond of the acetylene molecule forming t -INT1, t -INT2, and t -INT3. These collision complexes can isomerize to each other via barriers located well below the energy of the separated reactants; note that all three intermediates only weakly bound by 160 kJmol^{-1} to 180 kJmol^{-1} . The postulated inherent indirect scattering dynamics are also supported by the experimentally found center-of-mass angular distributions of this micro channel depicting intensity over the full angular range from 0° to 180° (section 4.4). Among the three initial collision complexes, only t -INT3 can lose a hydrogen atom via a tight transition state located about 26 kJmol^{-1} above the separated products to form the experimentally observed 1,3-butadiynyl radical plus atomic hydrogen; t -INT1 and t -INT2 have to rearrange to t -INT3 first. The existence of an exit barrier is also reflected in the shape of the center-of-mass translational energy distributions (section 4.3). Here, a broad distribution maxima of the $P(E_T)$ s extending up to 17 kJmol^{-1} from zero translational energy is evident. Recall that actually the flat plateau accounts for the nature of the exit transitions states in both reaction pathways on the singlet and triplet surfaces: a loose transition state peaking close to zero translation energy (micro channel 1) and a tight transition state depicting a maximum away from zero translational energy (micro channel 2). The latter pathway also correlates nicely with a significant geometry change and hence inherent electron reorganization from the decomposing t -INT3 complex to the 1,3-butadiynyl radical. Here, our computations suggest $r(\text{H-C1}) = 108.3 \text{ pm}$, $r(\text{H-C2}) = 108.9 \text{ pm}$, $r(\text{C1-C2}) = 135.1 \text{ pm}$, $r(\text{C2-C3}) = 138.8 \text{ pm}$, and $r(\text{C3-C4}) = 127.9 \text{ pm}$ (t -INT3) compared to $r(\text{H-C1}) = 106.3 \text{ pm}$, $r(\text{C1-C2}) = 120.6 \text{ pm}$, $r(\text{C2-C3}) = 136.5 \text{ pm}$, and $r(\text{C3-C4}) = 121.1 \text{ pm}$ (1,3-butadiynyl). Note that although the reversed reaction between 1,3-butadiynyl and atomic hydrogen presets formally an atom-radical reaction, this reaction does not portray a simple recombination of two radical centers as found on the singlet surface (section 5.2.1), but rather an addition of the hydrogen atom to a carbon-carbon triple bond of the 1,3-butadiynyl radical. We can compare the order of magnitude of the barrier to addition as found experimentally (about 17 kJmol^{-1}) and computationally (26 kJmol^{-1}) with a related system, i.e. the addition of atomic hydrogen to the carbon-carbon triple bond of acetylene, $C_2H_2(X^1\Sigma_g^+)$.¹²⁹ Here, the barrier of 19.7 kJmol^{-1} compares favorably well with the 1,3-butadiynyl plus atomic hydrogen reaction.

Having identified the feasible collision complexes (t-INT1, t-INT2, and t-INT3) and also the fragmenting intermediate to form the 1,3-butadiynyl radical plus atomic hydrogen (t-INT3), we propose now the underlying reaction dynamics of this micro channel. The dynamics have to account for the change of the center-of-mass angular distribution and the contour flux maps from a forward-scattered distribution to backward scattered distributions as the collision energy rises (sections 4.4 & 4.5). Since our calculations suggest that the reaction of dicarbon with acetylene on the triplet surface has no entrance barrier, the simple orbiting model predicts a decrease of the maximum reactive impact parameter as the collision energy increases.¹²⁶ In other words, at low collision energies, large impact parameters should dominate. Based on the geometric structures of the triplet intermediates t-INT1, t-INT2, and t-INT3, both latter structures should be favorably formed from dicarbon molecules holding large impact parameters (low collision energies). This would lead to a forward-scattered distribution of the 1,3-butadiynyl radical with respect to the dicarbon beam. On the other hand, small impact parameters at higher collision energies are expected to yield predominantly t-INT1; in the limiting case, the dicarbon molecule would collide with zero impact parameter under C_{2v} symmetry with the center-of-mass of the acetylene molecule; this would be reflected in a backward scattering of the 1,3-butadiynyl radical with respect to the dicarbon beam. Due to angular momentum conservation, the reduced impact parameter should go hand in hand with a diminishing total angular momentum \mathbf{J} . On the triplet surface, this in turn would result in less rotational excitation of the 1,3-butadiynyl radical as the collision energy increases (equations (13)-(16)). Summarized, the experimentally found switch from a forward to backward scattered flux contour maps can be reasonably understood in terms of an impact-parameter dictated reaction dynamics of barrier-less entrance channels, i.e. an initial formation of t-INT2 and t-INT3 at lower collision energies and inherent larger impact parameters and a preferential collision complex t-INT1 as the collision rises and the maximum impact parameter decreases. We would like to stress that although the reaction on the singlet and on the triplet surface yield the 1,3-butadiynyl radical, the rovibrational excitation on both surfaces is expected to differ significantly in channel 1 and 2. Recall that in a hypothetical crossed beam reaction of singlet dicarbon with $^{13}\text{C}_2\text{H}_2(\text{X}^1\Sigma_g^+)$, this reaction would yield $\text{H}^{13}\text{CC}^{13}\text{CC}(\text{X}^2\Sigma^+)$ and $\text{HC}^{13}\text{CC}^{13}\text{C}(\text{X}^2\Sigma^+)$ isotopomers via an initial addition, ring opening and hence formal insertion of one of the dicarbon carbon atoms into the carbon-carbon triple bond of the acetylene molecule (section 5.2.1.). However, on the triplet surface, dicarbon is found to be connected

‘end on’ to only one acetylenic carbon atom the decomposing intermediate t-INT3. This would provide solely the $\text{HCC}^{13}\text{C}^{13}\text{C}(\text{X}^2\Sigma^+)$ isotopomer on the triplet surface. Therefore, due to the distinct nature of the exit barriers (loose versus tight transition state on the singlet and triplet surfaces, respectively), the 1,3-butadiynyl radical formed on the triplet surface should have an enhanced vibrational excitation of the HCCC bending (ν_5 , ν_6 , and $\nu_7 = 576$, 376 , and 179 cm^{-1} , respectively) and of the $\text{C}\equiv\text{C}$ stretching modes (ν_2 and $\nu_3 = 2296$ and 2129 cm^{-1})¹⁷ compared to its counterpart synthesized on the singlet manifold.

The rotational motions of the prevailing triplet C_4H_2 complexes are very interesting. Similar to the singlet surface, the linear 1,3-butadiynyl radical must be excited to B-like rotations. Based on the rotational constants of $A = 44514.9 \text{ MHz}$, $B = 5714.3 \text{ MHz}$, and $C = 5064.2 \text{ MHz}$, the decomposing intermediate t-INT3 can be classified as a highly prolate rotor with asymmetry parameter $\kappa = -0.97$. Accounting for angular momentum and energy conservation, t-INT3 can be excited to B and/or C-like rotations. A-like rotations can be ruled out since due to energy conservation only about 1 % of all t-INT3 intermediates can populate A-like rotations.¹³⁰ Also, A-like rotations of t-INT3 would result in rotations of the 1,3-butadiynyl radical around its intermolecular axis; these are, however, energetically not accessible. Figure 11 compiles the feasible rotations of t-INT3. Note that C-like rotations of t-INT3 could result in an ejection of the hydrogen atom almost parallel to the total angular momentum vector. Therefore, the mildly sideways scattering as shown in the contour plots at lower collision energies could be the result of t-INT3 complexes excited to B-like rotations.

We would like to address briefly the possibility of the involvement of excited triplet surfaces and the potential involvement of an excited state of the 1,3-butadiynyl radical, $\text{C}_4\text{H}(\text{A}^2\Pi)$. In the entrance channel, $\text{C}_2(\text{a}^3\Pi_u)$ splits into $^3\text{A}'$ and $^3\text{A}''$ if the reaction takes place under C_s symmetry. Which surface is lower in symmetry, depends on the particular structure of the intermediate. In the entrance channel, $^3\text{A}''$ is lower in energy, because, although the t-INT2 and t-INT3 structures slightly deviate from the planarity and have a ^3A electronic state in C_1 symmetry, they correlate with the planar C_s -symmetric structures with a $^3\text{A}''$ state possessing one imaginary frequency, and the electronically excited $^3\text{A}'$ structures lie about 40 kJmol^{-1} higher in energy. Also, t-INT1

has a 3A_2 electronic state which correlates with a ${}^3A''$ state in C_s . However, if no symmetry is conserved (as it is the case for this reaction since t-INT3 belongs to the C_1 point group), the lowest energy surface of the $C_2(a^3\Pi_u) + C_2H_2(X^1\Sigma_g^+)$ reaction correlates with the lowest triplet state of all C_4H_2 isomers (3A); the higher energy surface would correlate to the first excited triplet states of all C_4H_2 intermediates. Based on these considerations, $C_4H(A^2\Pi)$ could be formed on an excited 3A under C_1 symmetry. However, our experimental data – particularly the exoergicities and the dynamics of the reaction – suggests that the 1,3-butadiynyl radical should be synthesized in its electronic ground state.

Finally, it is important to discuss the possibility to eliminate molecular hydrogen on the triplet surface. Here, the $C_4(X^3\Sigma_g^-) + H_2(X^1\Sigma_g^+)$ products lie 10.1 kJmol^{-1} below the reactants; the potential precursors for molecular hydrogen elimination are $CHCHCC$ (t-INT2), H_2CCCC (t-INT9), and $HCCCCH$ (t-INT7). However, we were able to locate a molecular hydrogen loss transition state only from the latter. This transition state has a six-member ring structure and lies very high in energy, 190.5 kJmol^{-1} above $C_2(a^3\Pi_u) + H_2(X^1\Sigma_g^+)$ (Figure 9). Thus, the forward and reverse barriers for $H_2(X^1\Sigma_g^+)$ elimination from t-INT7 are 450.7 and 200.6 kJmol^{-1} ; and this channel is very unfavorable. The search of transition state for the $H_2(X^1\Sigma_g^+)$ losses from t-INT9 and t-INT2 converges to a transition state, which - according to intrinsic reaction coordinate calculations - actually corresponds to the hydrogen atom abstraction reaction, $HCCCCH(X^2\Sigma^+) + H({}^2S_{1/2}) \rightarrow C_4(X^3\Sigma_g^-) + H_2(X^1\Sigma_g^+)$. This means that a $H_2(X^1\Sigma_g^+)$ elimination from t-INT9 and t-INT2 is unfavorable as compared to the two-step process, i.e. the elimination of a hydrogen atom followed by hydrogen abstraction from the 1,3-butadiynyl radical by the hydrogen atom produced at the first step. Therefore, the $C_4(X^3\Sigma_g^-) + H_2(X^1\Sigma_g^+)$ products can only be formed through secondary reactions of the 1,3-butadiynyl radical with hydrogen atoms, which is not possible under single collision conditions. This correlates nicely with the failed detection of molecular hydrogen in the crossed beams experiments. The hydrogen abstraction barrier is calculated to be 89.5 and 59.2 kJmol^{-1} relative to $C_4H(X^2\Sigma^+) + H({}^2S_{1/2})$ and $C_4(X^3\Sigma_g^-) + H_2(X^1\Sigma_g^+)$, respectively. If we consider the reverse reaction of $C_4(X^3\Sigma_g^-)$ with $H_2(X^1\Sigma_g^+)$, tetracarbon can be looked at as a σ -radical, similar to $C_2H_3(X^2A')$, $C_2H(X^2\Sigma^+)$, or $HCCCCH(X^2\Sigma^+)$. We have demonstrated earlier,¹³¹ on the basis of the molecular orbital consideration, that $H_2(X^1\Sigma_g^+)$ addition to such σ -radi-

cal is not possible; all of them prefer to react with molecular hydrogen by hydrogen abstraction. This also makes the reverse reactions of a molecular hydrogen elimination unlikely since an atomic hydrogen loss followed by a hydrogen abstraction is more favorable.

5.3. Undetected Channels

Table 2 compiles the energetics of alternative exit channels. It is evident that the competing exit channels (3)–(6) are too endoergic to be relevant even at the highest collision energy of 47.5 kJmol⁻¹ as employed in the present study. Based on the energetics, the formation of two ethynyl radicals (channel (6)) might show minor contribution in the high energy tail of the Maxwell Boltzmann distribution in high temperature flames (5,000 K). In the triplet electronic state, dicarbon can also react with acetylene via hydrogen abstraction through direct scattering dynamics producing C₂H(X²Σ⁺)+C₂H(X²Σ⁺). Considering the reaction of triplet dicarbon with ¹³C₂H₂ (X¹Σ_g⁺), we expect to form only CCH(X²Σ⁺) + ¹³C¹³CH(X²Σ⁺). The barrier for this abstraction process is calculated to be rather high, 109.9 kJmol⁻¹. However, a direct hydrogen abstraction is not possible in the ground singlet state. Here, the C₂(X¹Σ_g⁺) addition to the acetylene molecule is a much more favorable process. The abstraction pathway in the singlet state might be possible if we consider an excited open-shell singlet surface. Using transition state search for the open-shell singlet ¹A" state, we were able to locate a stationary point corresponding to the hydrogen abstraction process. However, this structure has two imaginary frequencies and lies about 25 kJmol⁻¹ higher in energy (at the B3LYP level without zero point energy) than the hydrogen abstraction transition state in the triplet state and correlates to the excited state of the C₂H(X²Σ⁺) + C₂H(A²Π) products. We can conclude here that the direct hydrogen abstraction process to form ethynyl radicals is not possible under present experimental conditions on the singlet surface. Nevertheless, we identified the diacetylene molecule (s-INT3) as the decomposing intermediate to form 1,3-butadiynyl plus atomic hydrogen. On the other hand, diacetylene could undergo a carbon-carbon single bond rupture producing C₂H(X²Σ⁺) + C₂H(X²Σ⁺). In this scenario, the formation of the ethynyl radical presents proceeds through indirect scattering dynamics; in a reaction of singlet dicarbon with ¹³C₂H₂(X¹Σ_g⁺), we would expect solely C¹³CH (X²Σ⁺) + ¹³CCH(X²Σ⁺) to be synthesized. Nevertheless, the overall energetics should favor the hydrogen

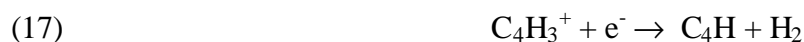
elimination pathway from s-INT3 compared to the carbon-carbon bond rupture process. As a matter of fact, in our crossed beams experiments, reaction (6) is too endoergic to proceed.

Table 2. Reaction enthalpies of exit channels of the $C_2(X^1\Sigma_g^+) + C_2H_2(X^1\Sigma_g^+)$ reaction.

	products	reaction enthalpy, kJmol^{-1}
1	$C_4H(X^2\Sigma^+) + H(^2S_{1/2})$	- 33
2	$C_4(X^3\Pi_u) + H_2(X^1\Sigma_g^+)$	-3
3	$c\text{-}C_3H_2(X^1A_1) + C(^3P_j)$	+ 152
4	$c\text{-}C_3H(X^2B_1) + CH(X^2\Pi)$	+ 246
5	$CH_2(X^3B_1) + C_3(X^1\Sigma_g^+)$	+ 142
6	$C_2H(X^2\Sigma^+) + C_2H(X^2\Sigma^+)$	+ 73

6. Implications to Astrochemistry

The explicit identification of the 1,3-butadiynyl radical, $C_4H(X^2\Sigma^+)$, in the crossed beam reaction of dicarbon molecules $C_2(X^1\Sigma_g^+/a^3\Pi_u)$, with acetylene, $C_2H_2(X^1\Sigma_g^+)$, presents compelling evidence that the 1,3-butadiynyl radical can be formed via bimolecular reactions involving carbon clusters in circumstellar envelopes of dying carbon stars. Competing ion-molecule reaction schemes (1)-(2) and (17)-(18) have been proposed to form 1,3-butadiynyl in circumstellar envelopes and in cold molecular clouds, but an incorporation of these reactions into interstellar reaction networks failed to reproduce the column density of astronomically observed 1,3-butadiynyl radicals.¹³² Therefore, since acetylene and dicarbon molecules are highly abundant in, for instance, the circumstellar shell of IRC+10216 at temperatures of up to a few thousand Kelvin, our study suggests that neutral gas phase reactions of singlet dicarbon molecules are of potential importance. Also, the absence of any entrance barrier suggests that this process also can form 1,3-butadiynyl radicals in cold molecular clouds where temperatures as low as 10 K prevail. The reaction of dicarbon in its triplet state is also of potential relevance to the cometary chemistry community, since $C_2(a^3\Pi_u)$ has been identified in close proximity to, for instance, P/Halley's nucleus in the gas phase.



7. Implications to Combustion Processes

The reaction dynamics of pure carbon molecules are of increasing interest not only due to their crucial role in astrochemistry, but also in combustion processes due to their potential importance in the synthesis of hydrogen-deficient precursors of polycyclic aromatic hydrocarbons (PAHs), fullerene, and soot particles. The crossed molecular beams studies did not only identify the 1,3-butadiynyl radical plus atomic hydrogen as the sole reaction channel, but also provided important information of the intermediates involved. These are singlet and triplet INT1, INT2, and INT3. Under single collision conditions as prevailing in cold molecular clouds and in the outer regions of the circumstellar envelopes of aging carbon stars, these reaction intermediates cannot be stabilized, and hence they fragment to the products or react back to the reactants. However, the higher density of the reactant as well as bath molecules – predominantly molecular nitrogen – in combustion flames allows a collision-induced stabilization of the reaction intermediates (three body processes) to become more increasingly important. Therefore, future spectroscopic probes of sooting hydrocarbon flames should also try to detect spectral signatures of the INT1, INT2, and INT3 intermediates. Recall, for instance, that Kubitzka et al. trapped unstable radicals in combustion flames via dimethyldisulfide by freezing the scavenged radical intermediates as methylthioethers at 77 K.¹³³ This led not only to the actual detection of the 1,3-butadiynyl radical, but also to the identification of various hitherto poorly characterized C₄H₂ intermediates – among them diacetylene s-INT3 - in oxygen-deficient acetylene and benzene flames.¹³⁴

8. Conclusions

We investigated the reaction of dicarbon molecules in their electronic ground, C₂(X¹Σ_g⁺), and first excited state, C₂(a³Π_u), with acetylene, C₂H₂(X¹Σ_g⁺), to form the 1,3-butadiynyl, C₄H(X²Σ⁺), plus a hydrogen atom under single collision conditions at six different collision energies between 10.6 kJmol⁻¹ and 47.5 kJmol⁻¹. The crossed molecular beam experiments were augmented with electronic structure calculations on the singlet and triplet C₄H₂ potential energy surfaces. On the singlet surface, dicarbon was found to react with acetylene on the ¹A surface without entrance barrier through an indirect reaction mechanism via an addition process through an initial s-INT1 and/or s-INT2 complex(es); both structures can be interconverted. The s-INT2 intermediate ring

opens to form the diacetylene molecule s-INT3 which is residing in a deep potential energy well. The latter decomposes via a loose exit transition state by an emission of a hydrogen atom to form the 1,3-butadiynyl radical $C_4H(X^2\Sigma^+)$; the overall reaction was found to be exoergic by about 33 kJmol^{-1} . The $D_{\infty h}$ symmetry of the decomposing diacetylene intermediate results in collision-energy invariant, isotropic (flat) center-of-mass angular distributions of this microchannel. On the triplet surface, the reaction involved three feasible addition complexes t-INT1, t-INT2, and t-INT3. Following the 3A surface, the reaction strongly depends on the impact parameter. Lower collision energies go hand-in-hand with larger impact parameters and hence the formation of t-INT2 and t-INT3 as the initial collision complex, whereas with increasing collision energy, smaller impact parameters and hence the involvement of t-INT1 becomes more important. All three initial collision complexes are located in shallower potential energy wells as compared to diacetylene on the singlet surface. These dynamics result in forward-scattered contour plots of the heavy 1,3-butadiynyl radical $C_4H(X^2\Sigma^+)$ at lower collision energies; as the collision energy rises, the distributions switch to a pronounced backward scattering. The definite detection of the 1,3-butadiynyl radical, $C_4H(X^2\Sigma^+)$, as the sole reaction product of the dicarbon versus hydrogen exchange pathway in the bimolecular collision with acetylene underlines the importance of this reaction not only in astrochemistry, but also in combustion scenarios. Here, we also identified six C_4H_2 intermediates which can be stabilized in combustion flames via tree body reactions.

ACKNOWLEDGMENTS

The experimental and theoretical work was supported by the US Department of Energy-Basic Energy Sciences (DE-FG02-03ER15411 and DE-FG02-04ER15570, respectively; the construction of the crossed beams machine was also aided by the National Science Foundation (CHE-0234461).

References

- ¹ Heath, J.R. in Fullerenes, G.S. Hammond, V.J. Kuck, Eds., American Chemical Society, Washington (1992).
- ² Minh, Y.C.; van Dishoeck, E.F. Astrochemistry: From Molecular Clouds to Planetary Systems. Astronomical Society of the Pacific, San Francisco (2000).
- ³ Millar, T.J.; Farquhar, P.R.A.; Willacy, K. Astron. Astrophys. Suppl. Series 1997, 121, 139.
- ⁴ Doty, S.D.; Leung, C.M. ApJ 1998, 502, 898.
- ⁵ Faraday Discussions 109, Chemistry and Physics of Molecules and Grains in Space (1998).
- ⁶ Sykes, M.V. The Future of Solar System Exploration. Astronomical Society of the Pacific, San Francisco (2002).
- ⁷ Summers, M.E.; Strobel, D.F. ApJ 1989, 346, 495.
- ⁸ Kiefer, J.H.; Sidhu, S.S.; Kern, R.D.; Xie, K.; Chen, H.; Harding, L.B. Combustion Science and Technology 1992, 82, 101.
- ⁹ Hausmann, M.; Homann, K.H. International Annual Conference of ICT (1991), 22nd (Combustion React. Kinetics) 1.
- ¹⁰ Zhang, H.Y.; McKinnon, J.T. Combustion Science and Technology 1995, 107, 261.
- ¹¹ Dismuke, K.I.; Graham, W.R.M.; Weltner, W., Jr. Journal of Molecular Spectroscopy 1975, 57, 127.
- ¹² Jacox, M.E., Journal of Physical and Chemical Reference Data 1990, 19, 1387.
- ¹³ Shen, L. N.; Doyle, T. J.; Graham, W.R.M. Journal of Chemical Physics 1990, 93, 1597.
- ¹⁴ Jacox, Marilyn E. Journal of Physical and Chemical Reference Data 1984, 13, 945.
- ¹⁵ <http://webbook.nist.gov/chemistry/>
- ¹⁶ Hoshina, K.; Kohguchi, H.; Ohsima, Y.; Endo, Y. J. Chem. Phys. 1998, 108, 3465.
- ¹⁷ Graf, S.; Geiss, J.; Leutwyler, S. Journal of Chemical Physics 2001, 114, 4542.
- ¹⁸ Gottlieb, C. A.; Gottlieb, E. W.; Thaddeus, P.; Kawamura, H. Astrophysical Journal 1983, 275, 916.
- ¹⁹ Yamamoto, S.; Saito, S.; Guelin, M.; Cernicharo, J.; Suzuki, H.; Ohishi, M. Astrophysical Journal 1987, 323, L149.
- ²⁰ McCarthy, M. C.; Gottlieb, C. A.; Thaddeus, P.; Horn, M.; Botschwina, P. Journal of Chemical Physics 1995, 103, 7820.

-
- ²¹ Chen, W.; Novick, S.E.; McCarthy, M. C.; Gottlieb, C. A.; Thaddeus, P. *Journal of Chemical Physics* 1995, 103, 7828.
- ²² Woon, D.E. *Chemical Physics Letters* 1995, 244, 45.
- ²³ Golovin, A. V.; Takhistov, V. V. *Journal of Molecular Structure* 2004, 701, 57.
- ²⁴ Wing, R.F. *The Carbon Star Phenomenon*, International Astronomical Union, Kluwer (2000).
- ²⁵ Guelin, M.; Green, S.; Thaddeus, P. *Astrophysical Journal* 1978, 224, L27.
- ²⁶ Doty, S.D.; Leung, C.M. *ApJ* 1998, 502, 898.
- ²⁷ Dayal, A.; Bieging, J.H. *Astrophysical Journal* 1993, 407, L37.
- ²⁸ Cernicharo, J.; Guelin, M.; Kahane, C. *Astronomy & Astrophysics, Supplement Series* 2000, 142, 181.
- ²⁹ Irvine, W. M.; Hoglund, B.; Friberg, P.; Askne, J.; Ellder, J. *Astrophysical Journal* 1981, 248, L113.
- ³⁰ Friberg, P.; Hjalmarsen, A.; Irvine, W.M. *ApJ. Lett.* 1980, 241, L99.
- ³¹ Bell, M. B.; Feldman, P. A.; Watson, J. K. G.; McCarthy, M. C.; Travers, M. J.; Gottlieb, C. A.; Thaddeus, P. *Astrophysical Journal* 1999, 518, 740.
- ³² Kalenskii, S. V.; Slysh, V. I.; Goldsmith, P. F.; Johansson, L. E. B. *Astrophysical Journal* 2004, 610, 329.
- ³³ Hirota, T.; Maezawa, H.; Yamamoto, S. *Astrophysical Journal* 2004, 617, 399.
- ³⁴ Terzieva, R.; Herbst, E. *ApJ* 1998, 501, 207.
- ³⁵ Herbst, E. *Astrophysical Journal, Supplement Series* 1983, 53, 41.
- ³⁶ Bettens, R. P. A.; Herbst, E. *Astrophysical Journal* 1997, 478, 585.
- ³⁷ Morata, O.; Herbst, E. *European Space Agency, Special Publication SP-577*, 393 (2005).
- ³⁸ Pety, J.; Teyssier, D.; Fosse, D.; Gerin, M.; Roueff, E.; Abergel, A.; Habart, E.; Cernicharo, J. *Astrophysics* 2005, 14, 1.
- ³⁹ Teyssier, D.; Pety, J.; Gerin, M.; Fosse, D.; Abergel, A.; Roueff, E.; Joblin, C. *Springer Proceedings in Physics* 2004, 91, 521.
- ⁴⁰ Teyssier, D.; Fosse, D.; Gerin, M.; Pety, J.; Abergel, A.; Roueff, E. *Astronomy and Astrophysics* 2004, 417, 135.

-
- ⁴¹ Yung, Y.L.; deMore, W.B. *Photochemistry of Planetary Atmospheres*, Cambridge University Press, Cambridge (1999).
- ⁴² Stahl, F.; Schleyer, P.v.R.; Schaefer, H.F.; Kaiser, R.I. *Planetary and Space Science* 2002, 50, 685.
- ⁴³ Gladstone, G. Randall; Allen, Mark; Yung, Y. L. *Icarus* 1996, 119, 1.
- ⁴⁴ Taylor, S.R. *Solar System Evolution*, Cambridge University Press, Cambridge (2001).
- ⁴⁵ Summers, M.E.; Strobel, D.F. *Astrophysical Journal* 1989, 346, 495.
- ⁴⁶ Romani, P.N.; Atreya, S.K. *Icarus* 1988, 74, 424.
- ⁴⁷ Lorenz, R.; Mitton, J. *Lifting Titan's Veil*, Cambridge University Press, Cambridge (2002).
- ⁴⁸ Geiss, J.; Altwegg, K.; Balsiger, H.; Graf, S. *Space Science Reviews* 1999, 90, 253.
- ⁴⁹ Baukal, C.E. *Oxygen-enhanced combustion*. CRS Press, New York (1998).
- ⁵⁰ Faraday Discussion 119, *Combustion Chemistry: From Elementary Reactions to Macroscopic Processes* (2001).
- ⁵¹ Helling, C.; Joergensen, U. G.; Plez, B.; Johnson, H. R. *Astronomy and Astrophysics* 1996, 315, 194.
- ⁵² Frenklach, M.; Feigelson, E.D. *Astrophysical Journal* 1989, 341, 372.
- ⁵³ Hausmann, M.; Hebgén, P.; Homann, K.H. *Proceedings of the 24th Symposium (International) on Combustion*, 1992, 793.
- ⁵⁴ Pascoli, G.; Polleux, A. *AA* 2000, 359, 799.
- ⁵⁵ Luch K. et al. *Chemical Physics Letters* 2004, 385, 49.
- ⁵⁶ Dolgonos, G.A.; Pesherbe, G.H. *Int. J. Mass Spectr.* 2005, 241, 261.
- ⁵⁷ Dolgonos, G.A.; Pesherbe, G.H. *Chemical Physics Letters* 2004, 398, 217.
- ⁵⁸ Duran, R. P.; Amorebieta, V. T.; Colussi, A. J. *Journal of Physical Chemistry* 1988, 92, 636.
- ⁵⁹ Zhang, H.-Y.; McKinnon, J. T. *Combustion Science and Technology* 1995, 107, 261.
- ⁶⁰ Warnatz, J.; Maas, U.; Dibble, R.W.; *Combustion*, Springer, Berlin (2001).
- ⁶¹ Appel, J.; Bockhorn, H.; Frenklach, M. *Combust. Flame* 2000, 121, 122. Richter, H.; Howard, J.B. *Progress in Energy and Combustion Science* 2000, 26, 565.
- ⁶² Kazakov, A.; Frenklach, M. *Comb. Flame* 1998, 112, 270.
- ⁶³ Homann, K.H. *Angew. Chem. Int. Ed.* 1998, 37, 2434.

-
- ⁶⁴ Baird, C. Environmental Chemistry. W.H. Freeman Company, New York (1999).
- ⁶⁵ Finlayson-Pitts, B.J.; Pitts, J.N. Science 1997, 276, 1045.
- ⁶⁶ Wayne, R.P. Chemistry of the Atmosphere. Oxford University Press, Oxford (2000).
- ⁶⁷ Loewe, A.G.; Hartlieb, A.T.; Brand, J.; Atakan, B.; Kohse-Hoinghaus, K. Comb. Flames, 1999, 118, 37.
- ⁶⁸ Pety, J.; Teyssier, D.; Fosse, D.; Gerin, M.; Roueff, E.; Abergel, A.; Habart, E.; Cernicharo, J. Astronomy and Astrophysics 2005, 435, 885.
- ⁶⁹ Cernicharo, J.; Goicoechea, J.R.; Benilan, Y. ApJ Lett 2002, 580, 157.
- ⁷⁰ Nejad, L.A.M.; Millar, T.J. AA 1987, 183, 279.
- ⁷¹ Smith, I.W.M.; Herbst, E.; Chang, Q. Monthly Notices of the Royal Astronomical Society 2004, 350, 323.
- ⁷² Bettens, R.P.A.; Lee, H.H.; Herbst, E. ApJ 1995, 443, 664.
- ⁷³ Kaiser, R. I.; Balucani, N.; Charkin, D. O.; Mebel, A. M. Chem. Phys. Lett. 2003, 382, 112.
- ⁷⁴ Gordon, A.G. The Spectroscopy of Flames, Wiley, New York (1974). Clary, D.C. Annu. Rev. Phys. Chem. 1990, 41, 61.
- ⁷⁵ Yorke, S.B. Astrophys. J. 1983, 88, 1816.
- ⁷⁶ Combi, M.R.; Fink, U. Astrophys. J. 1997, 484, 879.
- ⁷⁷ Swamy, K.S.K. Astrophys. J. 1997, 481, 1004.
- ⁷⁸ Rousselot, P. ; Laffont, C. ; Moreels G.; Clairemidi, J. AA 1998, 335, 765.
- ⁷⁹ John, P. ; Rabeau, J.R. ; Wilson, J.I.B. Diam. Related Materials 2002, 11, 608.
- ⁸⁰ Baranovski, A.P. ; McDonalds, J.R. J. Phys. Chem. 1977, 66, 3300.
- ⁸¹ Smith, G.P. ; Park, C. ; Schneiderman, J.; Luque, J. Comb. Flame 2005, 141, 66.
- ⁸² Weltner, W. ; van Zee, R.J. Chem. Rev. 1989, 89, 1713.
- ⁸³ Rousselot, P.; Laffont C.; Moreels, G.; Clairemidi, J. AA 1998, 335, 765.
- ⁸⁴ Baranovski, A.P.; McDonalds, J.R. J. Phys. Chem. 1977, 66, 3300.
- ⁸⁵ Gredel, R. AA 1999, 351, 657.
- ⁸⁶ Kern, R.D.; Chen, H.; Kiefer, J.H.; Mudipalli, P.S. Combust. Sci. 1992, 85, 77. Frenklach, M. Phys. Chem. Chem. Phys. 2002, 4, 2028. Baukal, C.E. Oxygen-enhanced combustion. CRS Press, New York (1998).
- ⁸⁷ Yorke, S.B. ApJ 1983, 88, 1816.

-
- ⁸⁸ I.A. Crawford, M.J. Barlow, MNRAS, 2000, 311, 370.
- ⁸⁹ Goyette, A.N.; Matsuda, Y.; Anderson, L.W.; Lawler, J.E. J. Vac. Sci. Technol. A 1998, 16, 337.
- ⁹⁰ Shiomi, T.; Nagai, H.; Hiramatsu, M.; Nawata, M. Diam. Rel. Mat. 2001, 10, 388.
- ⁹¹ Hiramatsu, M.; Kato, K.; Lau C.H., Foord, J.S.; Hori, M. Diam. Relat. Materials 2003, 12, 365.
- ⁹² Pascoli, G.; Polleux, A. Astron. Astrophys. 2000, 359, 799.
- ⁹³ Hill, H.G.M.; Jones, A.P.; d'Hendecourt, L.B. Astron. Astrophys. 1998, 336, L41.
- ⁹⁴ Andersen, A.C.; Jorgensen, U.G.; Nicolaisen, F.M.; Sorensen, P.G.; Glejbol, K. Astron. Astrophys. 1998, 330, 1080.
- ⁹⁵ C.J. Rennick, J.A. Smith, M.N.R. Ashfold, A.J. Orr-Ewing, CPL 383 518 (2004).
- ⁹⁶ Winicur, D. H.; Hardwick, J. L.; Murphy, S. N. Combustion and Flame 1983, 53, 93.
- ⁹⁷ Chan M.C. et al. Chem Phys. Lett 2004, 390, 340.
- ⁹⁸ Doty, S.D.; Leung, C.X.M. ApJ 1998, 502, 898.
- ⁹⁹ Mebel A.M. et al. JCP 2001, 114, 9821.
- ¹⁰⁰ Blunt, V.M.; Lin, H.; Sorkhabi, O.; Jackson, W.M. CPL 1996, 257, 347.
- ¹⁰¹ Sherrill, C.D.; Piecuch, P. JCP 2005, 122, 124104.
- ¹⁰² Abrams, M.L.; Sherrill, C.D. JCP 2004, 121, 9211.
- ¹⁰³ Toffoli, D.; Lucchese, R.R. JCP 2004, 120, 6010.
- ¹⁰⁴ van Orden, A.; Saykally, R.J. Chem. Rev. 1998, 98, 2313.
- ¹⁰⁵ Weltner, W.; Van Zee, R.J. Chem. Rev. 1989, 89, 1713.
- ¹⁰⁶ Huang, C.; Hu, Z.; Xin, Y.; Pei, L.; Chen, Y. JCP 2004, 120, 2225.
- ¹⁰⁷ Wang, H.; Zhu, Z.; Zhang, S.; Pei, L., Chen, Y. CPL 2005, 407, 217.
- ¹⁰⁸ Martin, M. J. Photochem. Photobiology A 1992, 66, 263.
- ¹⁰⁹ Huang, C.; Zhu, Z.; Wang, H.; Pei, L.; Chen, Y. JPCA 2005, 109, 3921.
- ¹¹⁰ Savic, I.; Cermak, I.; Gerlich, D. Int. J. Mass Spectr. 2005, 240, 139.
- ¹¹¹ Reisler, H.; Mangir, M.S.; Wittig, C. JCP 1980, 73, 2280.
- ¹¹² Chaquin, P.; Scemama, A. Chemical Physics Letters 2004, 394, 244.
- ¹¹³ Havenith, R.W.A.; Lugli, F.; Fowler, P.W.; Steiner, E. Journal of Physical Chemistry A 2002, 106, 5703.

-
- ¹¹⁴ Mabry, J.; Johnson, R.P. *JACS* 2002, 124, 6497.
- ¹¹⁵ Guo, Y.; Gu, X.; Kawamura, E.; Kaiser, R.I. *Rev. Sci. Instr.* (submitted 2005).
- ¹¹⁶ Kaiser, R.I. et al. *Faraday Discussion* 2001, 119, 51.
- ¹¹⁷ Gu, X.; Guo, Y.; Kaiser, R.I. *Int. J. Mass Spectrometry* (submitted 2005).
- ¹¹⁸ Brink, G.O. *Rev. Sci. Instrum.* 1996, 37, 857.
- ¹¹⁹ Daly, N.R. *Rev. Sci. Instrum.* 1960, 31, 264.
- ¹²⁰ Becke, A.D., *J. Chem. Phys.* 1993, 98, 5648. Lee, C.; Yang, W.; Parr, R.G. *Phys. Rev. B* 1988, 37, 785.
- ¹²¹ Purvis G.D.; Bartlett, R.J. *J. Chem. Phys.* 1982, 1076, 1910.
- ¹²² Frisch M.J. et al., *GAUSSIAN 98, Revision A.7.*, Gaussian Inc., Pittsburgh, PA (1998).
- ¹²³ MOLPRO is a package of ab initio programs written by H.J. Werner and P.J. Knowles with contributions from J. Almlóf et al.
- ¹²⁴ Kaiser, R.I.; Ochsenfeld, C.; Head-Gordon, M.; Lee, Y.T.; Suits, A.G. *Science* 1996, 274, 1508(1996).
- ¹²⁵ Miller, W.B.; Safron, S.A.; Herschbach D.R. *Discuss. Faraday. Society* 1967, 44, 108.
- ¹²⁶ Levine, R.D; Bernstein, R.B. *Molecular Reaction Dynamics and Chemical Reactivity*, Oxford University Press, Oxford (1987).
- ¹²⁷ J. Takahashi, *Publ. Astron. Soc. Japan* 2000, 52, 401.
- ¹²⁸ Tanimoto, M.; Kuchitsu, K.; Morino, Y. *Bulletin of the Chemical Society of Japan* 1969, 42, 2519.
- ¹²⁹ Zhang, P.; Irle, S.; Morokuma, K.; Tschumper, G. S. *J. Chem. Phys.* 2003, 119, 6524.
- ¹³⁰ The detailed computational procedure can be found in Kaiser, R.I.; Lee, Y.T.; Suits, A.G. *J. Chem. Phys.* 1996, 105, 8705.
- ¹³¹ Kim, G.-S.; Nguyen, T. L.; Mebel, A. M.; Lin, S. H.; Nguyen, M. T. *J. Phys. Chem. A* 2003, 107, 1788. Mebel, A. M.; Morokuma, K.; Lin, M. C. *J. Chem. Phys.* 1995, 103, 3440. Kurosaki, Y.; Takayanagi, T. *J. Chem. Phys.* 2000, 113, 4060. Le, T. N.; Mebel, A. M.; R. I. Kaiser, *J. Comput. Chem.* 2001, 22, 1522.
- ¹³² Tuner, B.E.; Herbst, E.; Terzieva, R. *ApJ SS* 2000, 126, 427.
- ¹³³ Kubitz, C.; Schottler, M.; Homann, K. H *Berichte der Bunsen-Gesellschaft* 1987, 91, 695.

¹³⁴ Hausmann, M.; Hebgen, P.; Homann, K. H. Symposium (International) on Combustion, [Proceedings] (1992).